JTTEES 2:79-92

Spray Parameters and Particle Behavior Relationships During Plasma Spraying

M. Vardelle, A. Vardelle, and P. Fauchais

Using laser anemometry, laser fluxmetry, and statistical two-color pyrometry, the velocity, number flux, and surface temperature distributions of alumina and zirconia particles in dc plasma jets have been determined inflight for various spraying parameters. The flux measurements emphasized the importance of the carrier gas flow rate, which must be adjusted to the plasma jet momentum depending on the arc current, nozzle diameter, gas flow rate, and gas nature. It has also been shown that the particle trajectories depend both on the particle size and injection velocity distributions and that the position and tilting of the injector plays a great role. The particle size drastically influences its surface temperature and velocity, and for the refractory materials studied, only the particles below 45 μm in diameter are fully molten in Ar-H_2 (30 vol%) plasma jets at 40 kW. The morphology of the particles is also a critical parameter. The agglomerated particles partially explode upon penetration into the jet, and the heat propagation phenomenon is seriously enhanced, particularly for particles larger than 40 μm. The effects of the arc current and gas flow rate have been studied, and the results obtained in an air atmosphere cannot be understood without considering the enhanced pumping of air when the plasma velocity is increased. The Ar-He (60 vol%) and Ar-H_2 (30 vol%) plasma jets, when conditions are found where both plasma jets have about the same dimensions, do not result in the same treatment for the particles. The particles are not as well heated in the Ar-He jet compared to the Ar-H_2 jet. Where the surrounding atmosphere is pure argon instead of air (in a controlled atmosphere chamber), the radial velocity and temperature distributions are broadened, and if the velocities are about the same, the temperatures are higher. The use of nozzle shields delays the air pumping and increases both the velocity and surface temperature of the particles. However, the velocity increase in this case does not seem to be an advantage for coating properties.

1. Introduction

THERMOMECHANICAL properties of dc plasma-sprayed coatings depend, among other parameters,[1-5] on the molten state and velocity of particles upon impact on the substrate, which control their flattening and the cooling of the resulting splats. For a given particle, its velocity and temperature upon impact are linked on the one hand to the plasma jet parameters—gas nature, velocity and temperature distributions, and turbulent mixing with the surrounding atmosphere—and on the other to each particle trajectory in the plasma jet. The trajectory is controlled by the particle injection velocity, the position where it is injected, its nature, density, size, and morphology. Other than the number of parameters involved, the fact that the particles have size and injection velocity distributions that result in a trajectory distribution adds to the complexity. Thus, all of the injected particles have widely different momentum and temperature histories. These very different trajectories result in different heat treatments undergone by the particles, heat treatments that are also complicated by heat propagation and evaporation phenomena, which are enhanced by low thermal conductivity particles and high thermal conductivity plasma jets. Thus, the coating results from the piling up of very different splats.

Keywords: gas types, injection modes, particle size effects, particle temperature, particle velocity, review paper, spray parameters, torch design

M. Vardelle, A. Vardelle, and **P. Fauchais,** Laboratoire Matériaux Céramiques et Traitements de Surface, University of Limoges, France.

The aim of this article is to show through in-flight measurements[6,7] on oxide particles the influence on their velocity and temperature distributions of the different macroscopic parameters, such as carrier gas flow rate, injector (internal diameter), position and tilting toward or against the plasma flow, powder size distribution, arc current, size of plasma gun nozzle, plasma gas nature, flow rate, and surrounding atmosphere. Of course, in-flight measurements give only mean values, and the distribution of each measured parameter should be considered. For example, particularly for the temperature distribution that might be rather broad, a mean value significantly over the melting temperature, T_m, does not necessarily mean that all the particles have their temperature over T_m. Moreover, the particles whose surface temperature is below 2000 K do not give any signal and are not taken into account by the measuring device. Thus, the temperature measurements must be considered cautiously, and they only provide trends. In the following, all the results presented were obtained at atmospheric pressure with the plasma jet flowing in air, except for one case in which it is flowing in an argon atmosphere.

2. Particle Injection

2.1 *Influence of Particle Injection Momentum*

For a given plasma jet (nozzle diameter, power level, gas nature, and flow rate), the momentum of the injected particles has to be adapted to that of the plasma jet so that they travel in the hot zones of the jet. This is illustrated in Fig. 1, where for a given plasma jet, a given carrier gas (always Ar in the following), a given injector, and a given fused and crushed alumina powder

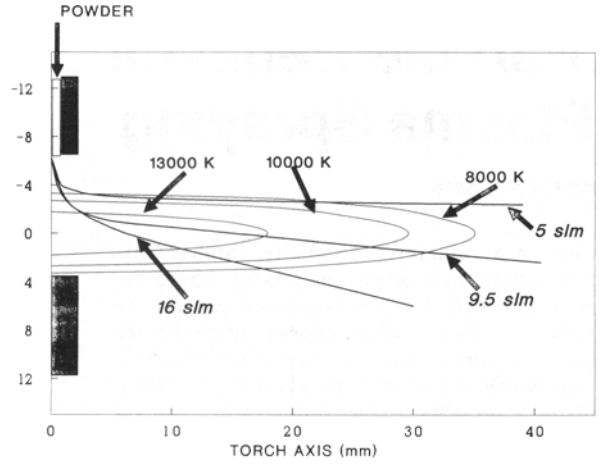

Fig. 1 Yttria-stabilized zirconia (8 wt% Y_2O_3) particle mean trajectory in an Ar-H_2 plasma jet. 75 slm Ar; 15 slm H_2; nozzle diameter, 8 mm; I = 450 A; V = 71 V; thermal efficiency ρ = 60%; fused and crushed powder –25+8 μm; injector inside diameter, 1.6 mm.

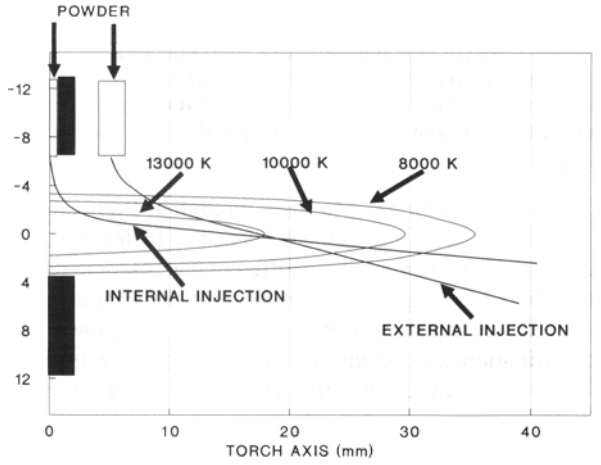

Fig. 2 Calcia-stabilized zirconia (7.5 wt% CaO) particle mean trajectory in an Ar-H_2 plasma jet. 75 slm Ar; 15 slm H_2; nozzle diameter, 8 mm; I = 450 A; V = 71 V; ρ = 60%; fused and crushed powder –15+5 μm; injector inside diameter, 1.6 mm.

size distribution, very different mean trajectories can be observed depending on the argon carrier gas flow rate. When the flow rate is too low, the particles do not penetrate into the jet, and when it is too high, they cross it. To illustrate the influence of the plasma jet momentum, Fig. 2 shows the trajectories obtained with the injector either in the nozzle, 3 mm upstream of its exit (internal injection), or outside, 5 mm downstream of its exit (external injection). The optimum trajectory is that corresponding to the highest surface temperature resulting in the highest deposition efficiency. With an internal injection, the optimum trajectory crosses the jet axis with an angle of about 3.5°. With the same carrier gas flow rate (9.5 slm) as that allowing an optimum trajectory with the internal injection, the particles cross the plasma jet more rapidly. This is due to the lower momentum of the expanding plasma jet. Similar results are obtained[8] if, for a given nozzle (ID = 7 mm) a given arc current (I = 500 A) and a given hydrogen volume percentage of 25%, the total flow rate,

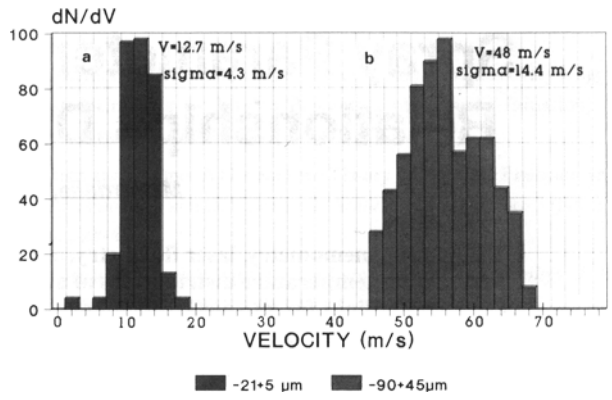

Fig. 3 Fused and crushed alumina particle injection velocity distributions corresponding to the same mean trajectory in an Ar-H_2 plasma jet. 75 slm Ar; 15 slm H_2; d = 8 mm; I = 400 A; V = 72 V; ρ = 60%; injector inside diameter, 1.6 mm. (a) –21+15 μm; $\dot{M}^{\circ}_{cg}$ = 7.5 slm. (b) –90+45 μm; $\dot{M}^{\circ}_{cg}$ = 2.5 slm.

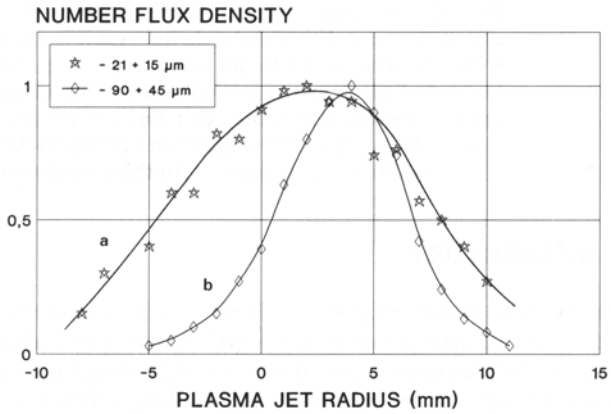

Fig. 4 Radial normalized number flux of fused and crushed particle in the Ar-H_2 plasma jet, defined in Fig. 3, measured 75 mm downstream of the nozzle exit for two size distributions. (a) –21+15 μm; $\dot{M}^{\circ}_{cg}$ = 7.5 slm. (b) –90+45 μm; $\dot{M}^{\circ}_{cg}$ = 2.5slm.

$\dot{m}^{\circ}$, of the plasma gas is increased. The carrier gas flow rate, $\dot{M}^{\circ}_{cg}$, must be increased correspondingly to obtain the same mean particle trajectory and thus the same mean deposition efficiency, ρ_D, as summarized in Table 1 for fused and crushed alumina particles (–45+22 μm).

The carrier gas flow rate corresponds to an injection velocity distribution. The smaller the particles, the higher the carrier gas flow rate and the higher the resulting velocities. This is illustrated[9] in Fig. 3 for fused and crushed alumina particles, which shows for two size ranges (–21+15 μm, left and –90 + 45 μm, right), the corresponding measured velocity distributions at the injector exit for two carrier gas flow rates giving the same mean trajectory. The important difference in the injection velocities for the two size distributions emphasizes the fact that the trajectories of the particles depend on their momentum. It should be noted that the velocities given in Fig. 3 were measured by laser doppler anemometry (LDA) in the direction of the injector axis. However, the radial velocity components are not at all negligible and correspond to a dispersion cone angle up to 30° for the small particles. Such a dispersion is due to the particle collisions with

the injector wall. The particle trajectories are thus the product of both size and injection velocity distributions.

It is not surprising that, even with a very narrow size distribution, the smaller particles, due to their very broad injection velocity distribution, exhibit a much broader trajectory distribution than the larger particles (Fig. 4) for which the velocity distribution is narrower. The distributions presented in Fig. 4 were measured in the direction parallel to the injector axis, but because of the nonaxial symmetry of this injection, a different distribution (broader) is obtained in a direction orthogonal to the injector axis. The maxima of these two number flux distributions define the "mean trajectory," as represented in Fig. 1 and 2.

Table 1 Correlation between the plasma gas flow rate and the carrier gas flow rate

Al_2O_3 particles –45+22 μm, fused and crushed, plasma gun nozzle, ID, 7 mm

$m°$, slm	46.7	53.3	60
P, kW	35	35	35
ρ_D, %	56	57	58
$\dot{M}°_{cg}$, slm	4.3	5.5	7

Of course, different trajectories resulting from different carrier gas flow rates induce[9] different velocity, v, surface temperature, T_s, and number flux radial distributions, as illustrated in Fig. 5(a), (b), and (c), respectively. The maximum v and T_s values correspond to $\dot{M}°_{cg}$ = 5.5 slm and a trajectory close to the jet axis (for example an angle of 3.5° between the jet axis and the mean trajectory as illustrated in Fig. 1). Of course, the highest values of T_s and v_s are obtained along the plasma jet axis.

2.2 *Influence of Powder Injector Tilting*

To increase the powder residence time in the plasma jet, it has been proposed to tilt the injector counter to the flow, as illustrated in Fig. 6. Similar mean trajectories[10] can be obtained with the two injectors by adjusting $\dot{M}°_{cg}$. If for the considered working conditions, $\dot{M}°_{cg}$ with the orthogonal injection, it then must be only 2 slm with the 60° injector, otherwise the mean trajectory crosses the plasma jet too rapidly. This tilting has a drastic influence on the mean velocity of the particle and temperature along their mean trajectory, as illustrated in Fig. 7(a) and (b). In spite of a higher velocity with the 60° counter current injection angle, the particles reach a higher surface temperature. This is due to the longer residence time of the particle in the hot-

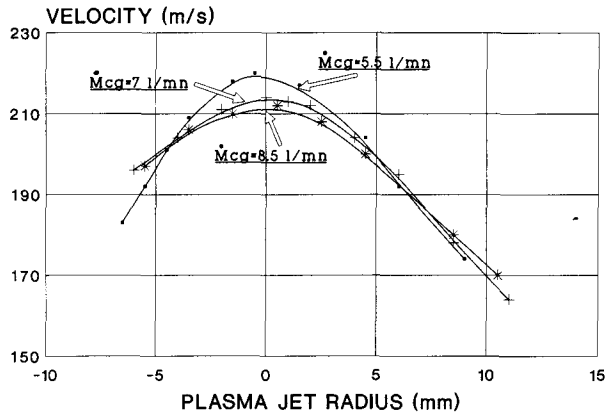

(a)

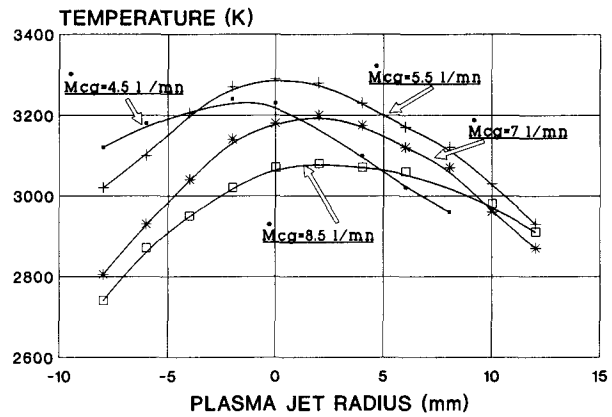

(b)

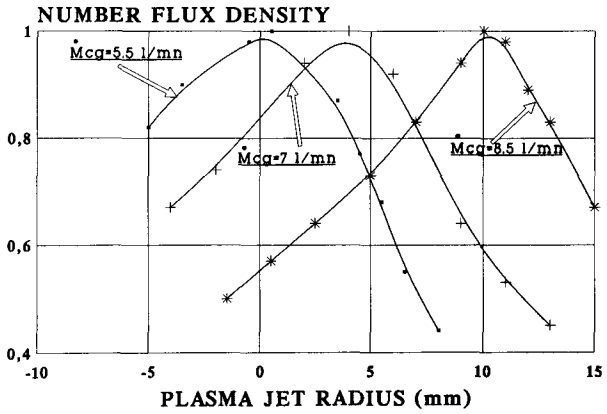

(c)

Fig. 5 Radial velocity (a), surface temperature (b), and number of flux distributions (c) for fused and crushed alumina particle –21+18 μm measured 75 mm downstream of the nozzle exit for different carrier gas flow rates in the plasma jet defined in Fig. 3.

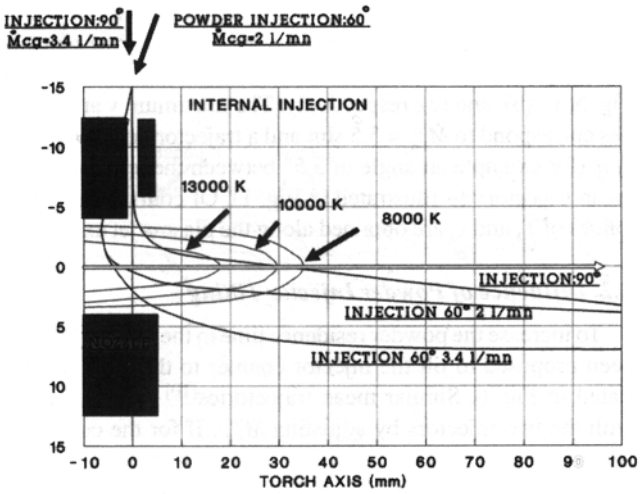

Fig. 6 Calcia-stabilized zirconia (7.5 wt% CaO) particle (–75+44 μm) mean trajectories for two injection angles (orthogonal to jet axis and 60° counter current) in the plasma jet defined in Fig. 3.

test zone of the jet. However, due to the lower injection velocity with the 60° angle and injection in a hotter zone of the plasma (compared to the 90° injection), problems occur where particles adhere and build up a deposit on the anode throat, thus reducing the interest in this type of injection.

3. Influence of Particle Size and Morphology

3.1 *Particle Size*

For similar trajectories and the same morphology, particle size plays an important role in the particle residence time in the hot zones of the plasma jet[5,11] and in the temperature that is reached. Surface temperature can be measured only outside of the plasma core,[6,7] as illustrated in Fig. 8 for fused and crushed alumina particles of –21 + 15 μm and –52 + 40 μm. The acceleration of the smaller particles is much higher (up to 70,000 g)

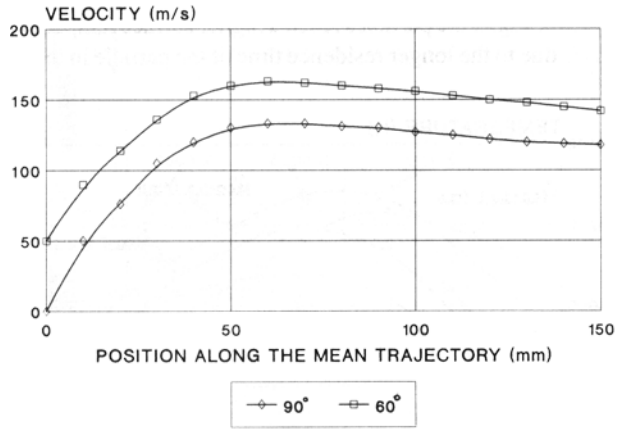

(a)

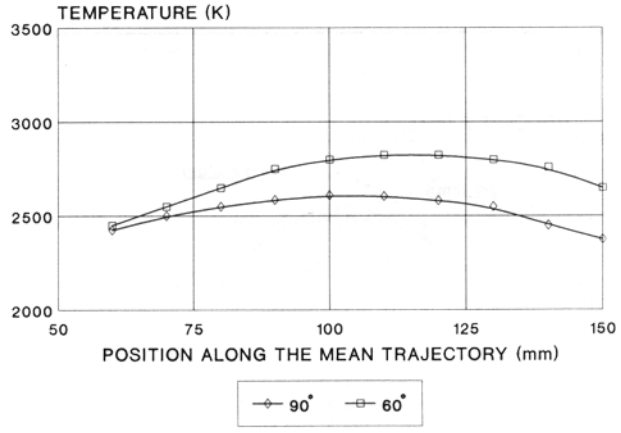

(b)

Fig. 7 Mean velocity (a) and surface temperature (b) along the mean trajectory of calcia-stabilized zirconia particles injected at 90 and 60° (see Fig. 6) in the plasma jet defined in Fig. 3.

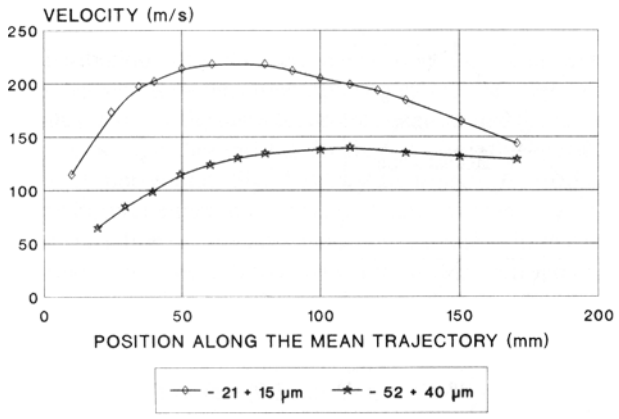

(a)

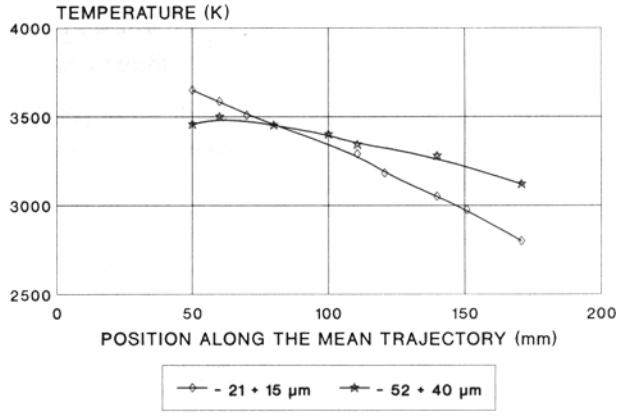

(b)

Fig. 8 Velocity (a) and surface temperature (b) along the same mean trajectory of fused and crushed alumina particles (–21+15 μm and –52+40 μm particle size range) injected in the Ar-H_2 plasma jet defined in Fig. 3.

than that of the larger ones (about 19,000 g). The maximum velocities are in a ratio of 1.7, but with their higher inertia the larger particles decelerate more slowly. For surface temperature, the maximum is reached for the larger particles only at the end of the plasma core (50 mm downstream of the nozzle exit) when at the same location the smaller particles are already cooling down. Similar velocity results were obtained with zirconia particles (stabilized with 8 wt% Y_2O_3) (Fig. 9). Because their density is about twice that of alumina, the maximum velocities for the same plasma jet are lower. However, for particles with such a low thermal conductivity (~1.5 W/m · K), surface temperature is not necessarily the mean temperature of the particle due to the heat propagation phenomenon.[12] With the argon/hydrogen plasma used, the Biot number varies between 0.06 and 0.2, and the center temperature, T_c, differs from the surface T_s, at least in the first few centimeters of the trajectory, as illustrated in Fig. 10. T_s and T_c have been calculated for two particle sizes with the same trajectory in the Ar-H_2 plasma jet used. Of course, T_s for the 60-μm particle is lower by 700 K than T_s for the 30-μm particle because heat propagation is slower. This means for example that, with the 60-μm particles, the substrate must be placed at least 80 mm downstream of the nozzle exit to receive completely molten particles upon impact (assuming the optimum trajectory!). Figure 10 also shows, at least for the 30-μm particle, that for distances greater than 70 mm the surface temperature decreases faster than the center temperature.

3.2 *Particle Morphology*

Even when particles have the same size distribution and the same chemical composition, they might have very different morphologies depending on the way they were manufactured.[13,14] For example, when comparing dense fused and crushed particles with porous agglomerated particles (agglomerates made with crushed particles in the size range –5+1 μm), very different results are obtained. If the fused and crushed par-

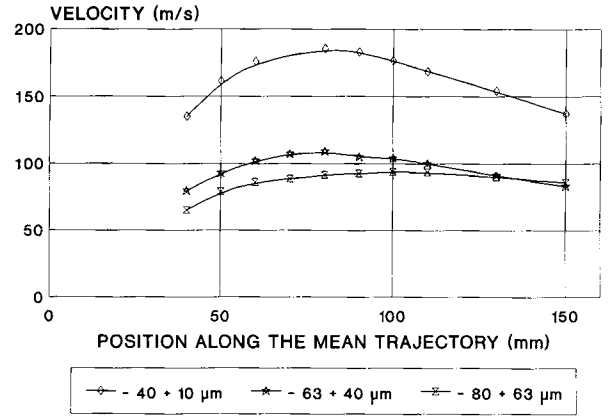

Fig. 9 Velocity of fused and crushed ZrO_2 + 8 wt% Y_2O_3 particles injected in the Ar-H_2 plasma jet defined in Fig. 3. The –40+10 μm particles were injected with a carrier gas flow rate ($\dot{M}_{cg}^{\circ}$) of 5.4 slm (V_{inj} = 17 m/s); the –63+40 μm particles with $\dot{M}_{cg}^{\circ}$ = 6.4 slm (V_{inj} = 13.3 m/s); the –80+63 μm particles with $\dot{M}cg$ = 4 slm (V_{inj} = 7 m/s).

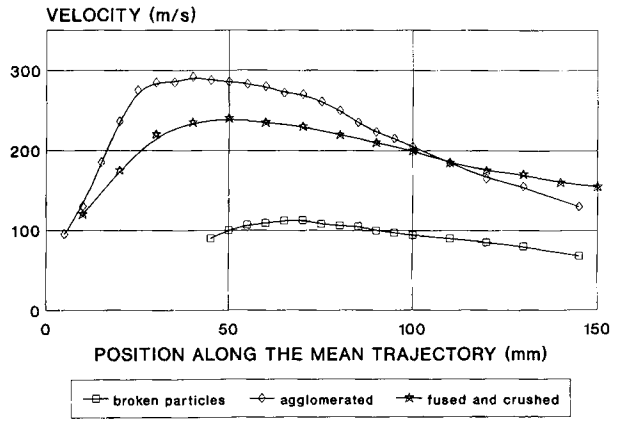

(a)

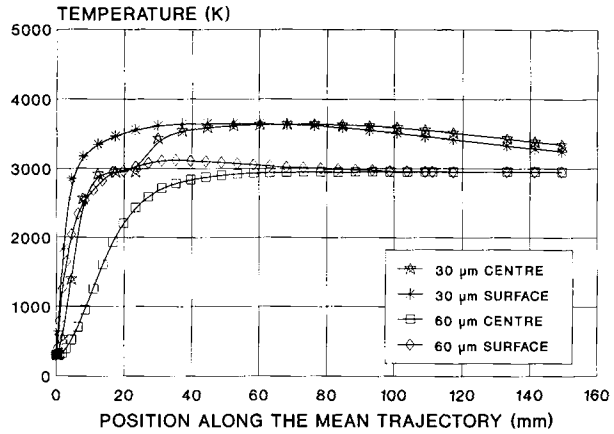

Fig. 10 Calculated surface and center temperatures of fused and crushed ZrO_2 + 8 wt% Y_2O_3 particles, 30 and 60 μm in diameter injected with the same trajectory in the Ar-H_2 plasma jet defined in Fig. 3.

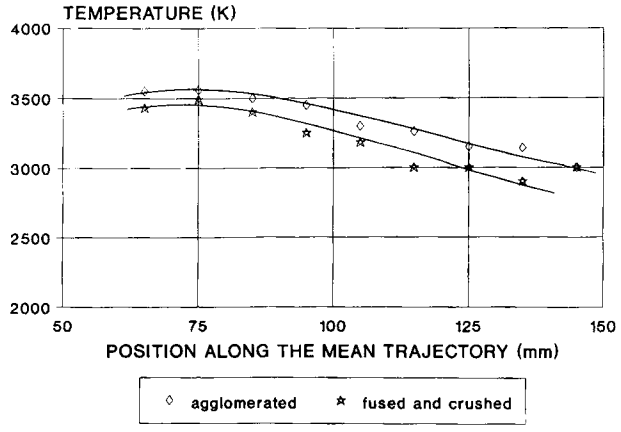

(b)

Fig. 11 Mean velocity (a) and surface temperature (b) along the mean trajectory of agglomerated and fused and crushed ZrO_2 + 8 wt% Y_2O_3 particles (–45+10 μm) injected in an Ar-H_2 plasma. 50 slm Ar; 15 slm H_2; nozzle diameter, 8 mm; P = 32 kW with carrier gas flow rates resulting in the same mean trajectory.

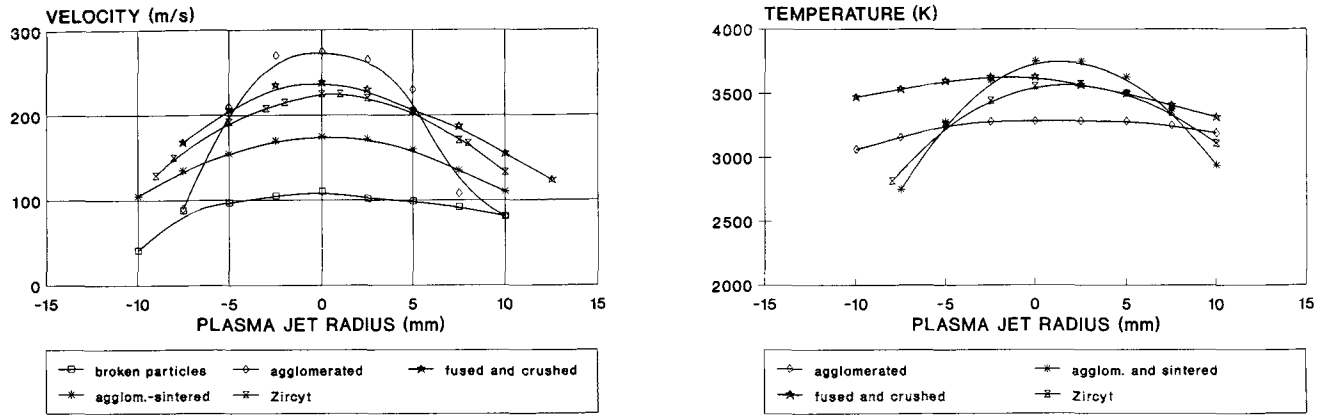

Fig. 12 Radial evolution of the velocity (a) and surface temperature (b) of –45+10 μm ZrO_2 + 8 wt% Y_2O_3 particles of different morphologies injected in the plasma depicted in Fig. 11. Measurements performed 75 mm downstream of the nozzle exit.

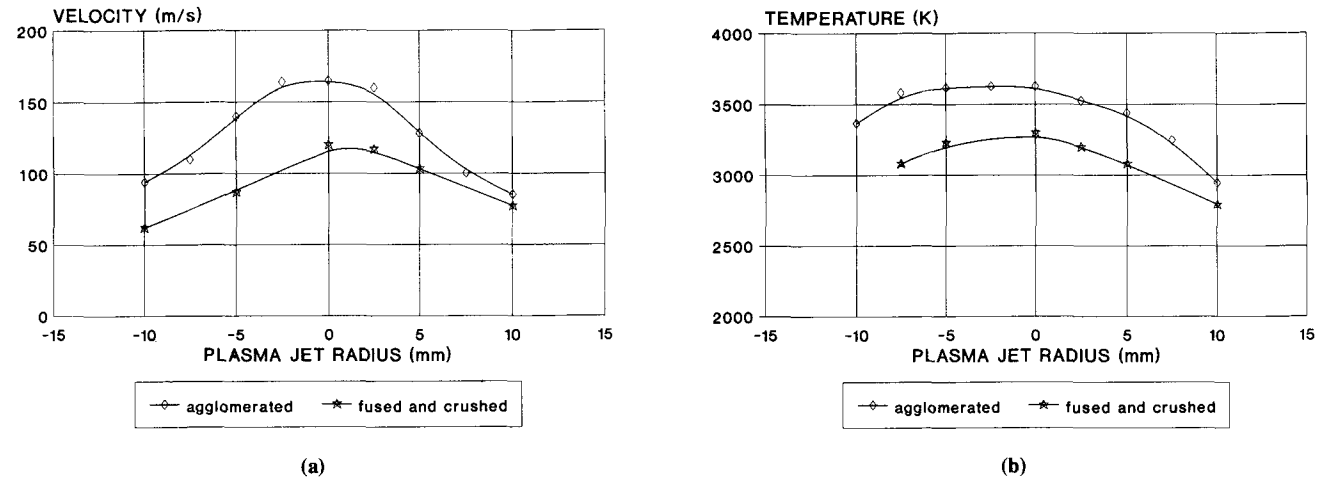

Fig. 13 Radial evolution of the velocity (a) and surface temperature (b) of –90+45 μm ZrO_2 + 8 wt% Y_2O_3 particles of different morphologies injected in the plasma depicted in Fig. 11. Measurements performed 75 mm downstream of the nozzle exit.

ticles exhibit normal behavior, the agglomerated particles partially explode upon penetration into the plasma jet. This is probably due to their poor mechanical resistance and the high thermal shock experienced when the gas trapped in the pore structure and the particles rapidly expand on exposure to the plasma jet. This is illustrated in Fig. 11(a), which shows three velocity distributions: that of the fused and crushed particles, that of the nonexploded agglomerated particles, and that of the exploded (or broken) agglomerated particles. The exploded particles do not penetrate into the jet because their momentum is too low; thus, they travel in its periphery and are dragged into the jet due to the large vortices created at the jet fringes. This results in a much lower velocity. According to their lower density (about half that of the fused and crushed particles) the agglomerated particles reach higher velocities than the fused and crushed particles, but they decelerate faster.

When considering the surface temperature, only two distributions are observed (see Fig. 11b). This is probably because the small exploded particles entrained in the low-temperature regions of the plasma do not reach 2000 K (which is the detection limit) or have been, because of their small size, heated in the jet plume to similar temperatures as that of the "large" particles that have crossed the hot core of the plasma jet. It is however interesting to note that T_s is higher for fused and crushed particles than for agglomerated particles, which is logical because the velocity of the fused and crushed particles is lower. Such results are confirmed by the particle radial distributions measured 75 mm downstream of the nozzle exit (see Fig. 12a and b). It is interesting to note that agglomerated and sintered particles whose density is between that of fused and crushed and agglomerated materials have similar temperatures as that of the fused and crushed particles (see Fig. 12b). "Zircyt" powders (ZrO_2 + 8 wt% Y_2O_3) that were made by a chemical route (the mean size of the agglomerates is about 0.1 μm versus a few micrometers for sintered or agglomerated particles) exhibit the same behavior (v and T_s) as that of the fused and crushed particles. It does not ap-

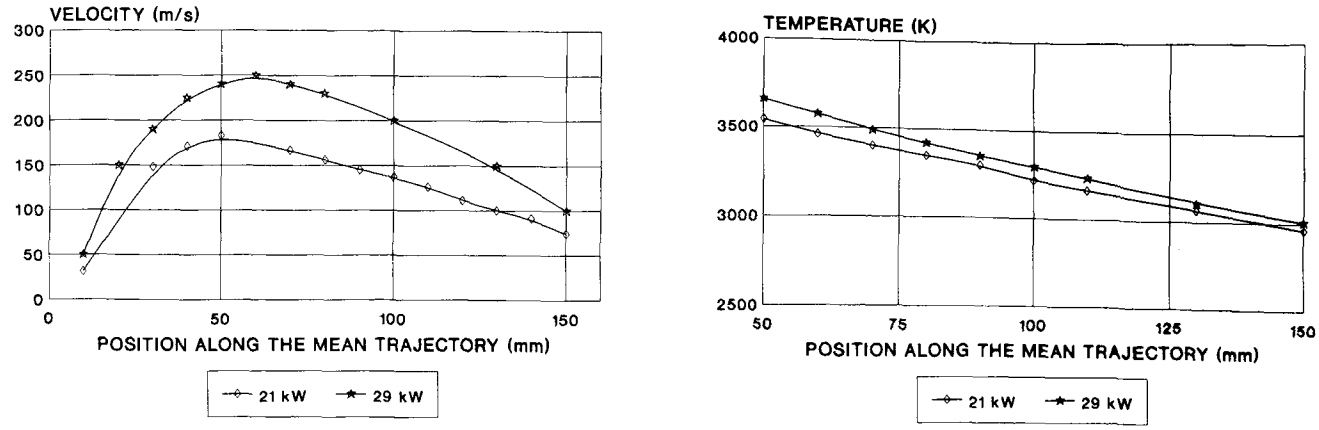

Fig. 14 Evolution along the mean trajectory of the velocity (a) and surface temperature (b) of fused and crushed alumina particles (–21+15 μm) injected in the plasma jet depicted in Fig. 3.

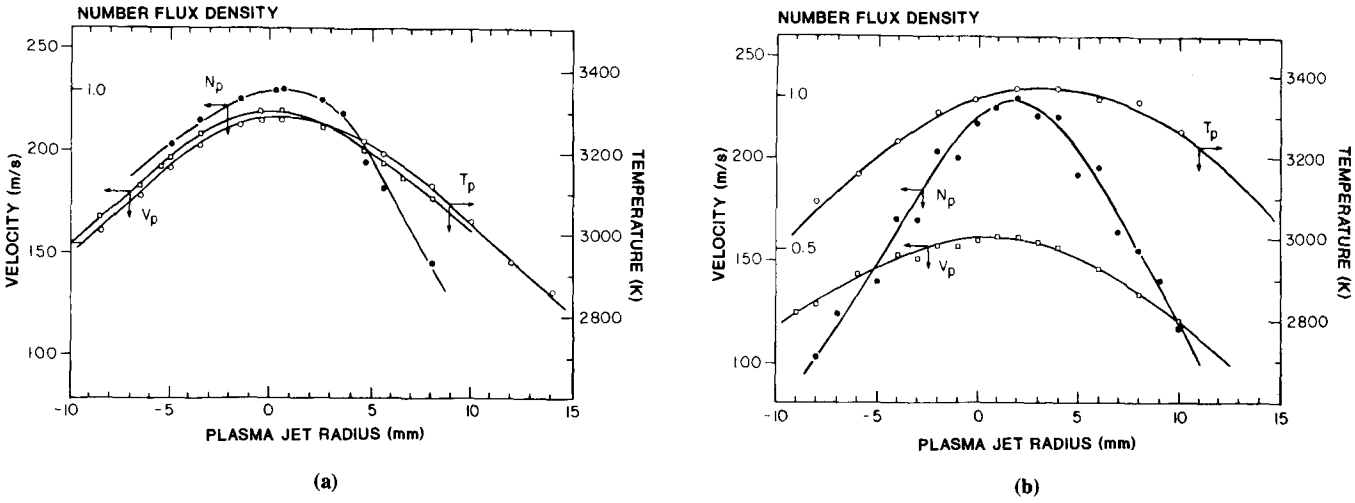

Fig. 15 Radial velocity, surface temperature, and normalized number flux distribution 75 mm downstream of the nozzle exit of fused and crushed alumina particles (–21+15 μm) injected in an Ar-H_2 plasma jet. Nozzle diameter, 8 mm; P = 29 kW. (a) Ar 45 slm, H_2 15 slm. (b) Ar 75 slm, H_2 15 slm.

pear that they explode upon penetration, but this size of elementary particles is about the detection limit of the authors' LDA setup.[6] Very different results were obtained when considering larger particles (–90 + 45 μm), as illustrated in Fig. 13 for fused and crushed and agglomerated particles. In this case, in spite of a higher velocity (see Fig. 13a), the agglomerated particles exhibit (see Fig. 13b) a higher surface temperature. The explanation can be found by looking at cross sections of the particles collected 200 mm downstream of the nozzle exit.[15] The –45 + 10 μm particles are uniformly porous, whereas the –90 + 45 μm particles are almost hollow spheres. The temperature of the small particles is 700 K higher than that of the large ones (see Fig. 10), whose temperature is hardly above the melting point. The gas trapped in the small porous agglomerated particles can escape through the liquid, whereas for the large particles it cannot because the temperature is very close to T_m. Consequently, the compressed gas expands the molten shell like a balloon. The surface temperature of the molten shell is thus overheated. Therefore, the best thermomechanical coating properties are obtained with the fused and crushed particles whose size is –45+10 μm.[16,17]

4. Influence of Spraying Parameters and Torch Design

As emphasized in a previous paper,[6] the influence of spraying parameters (arc current, I; gas flow rate, $m°$; gas nature) and torch design (nozzle diameter, nozzle shield) is rather complex. On the one hand, any parameter increasing the power level, such as I or H_2%, should increase both the length and velocity of the plasma jet. It is also the case that increasing the constriction of the plasma jet (e.g., with nozzle diameter decrease, mass flow rate increase, H_2% increase) increases the velocity. On the other

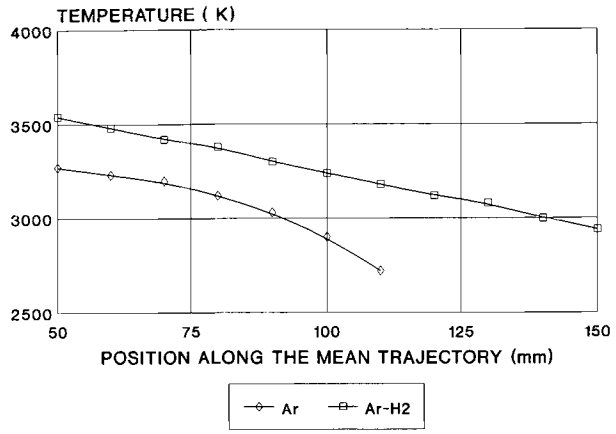

Fig. 16 Evolution along the mean trajectory of fused and crushed alumina particles (–21+18 μm) injected in a pure Ar plasma (13.3 kW) and in Ar-H_2 plasma (21 kW). Both plasmas had the same mean enthalpy.

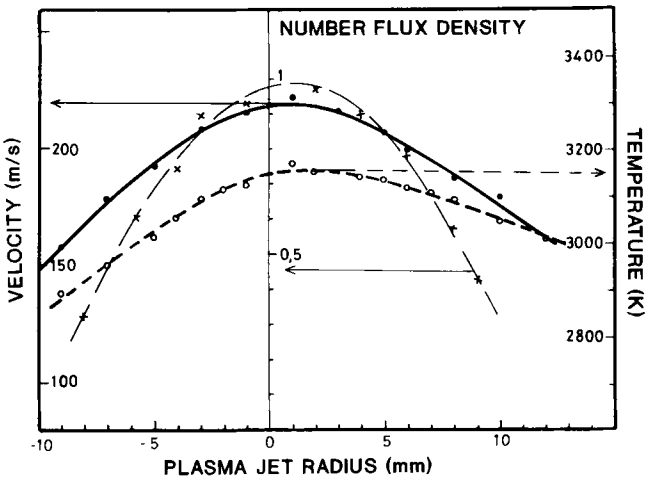

Fig. 17 Radial velocity, surface temperature, and normalized number flux distributions 75 mm downstream of the nozzle exit of fused and crushed alumina particles (–21+15 μm) injected in an Ar-H_2 plasma jet. Nozzle diameter, 8 mm; P = 29 kW; Ar 75 slm; H_2 7.5 slm.

hand, any increase in the plasma jet velocity enhances thermofluid interactions with the surrounding atmosphere[18] (known as pumping), which, when it is air, rapidly cools the plasma jet and reduces its length and diameter.[19] Moreover, the particle heating depends not only on the plasma enthalpy, but also on the thermal conductivity of the plasma gas, which is enhanced by the hydrogen or helium percentage in the plasma.

4.1 *Influence of Power Level*

The effect of an increase in power level is shown in Fig. 14. The shift from 21 to 29 kW was obtained by increasing the arc current. The maximum velocity of fused and crushed alumina particles increased by almost 40% when the temperature increase was less than 5%. This is due to the higher velocity of the plasma jet and to the fact that when increasing the power level by 40% the length of the plasma jet is only increased by 8%. This results in a shorter residence time and an enthalpy increase. It should be noted that when the surrounding atmosphere is argon then the length of the plasma jet increases with the arc current more regularly than in air. The limit of the plasma jet length reached at 700 A in air is not observed in an argon atmosphere. Thus, at least up to this arc current value, in argon atmosphere the increase in the surface temperature of the particles is almost linear with the arc current (see Fig. 11 in Ref 6).

4.2 *Influence of Plasma Gas Flow Rate*

Figure 15 shows radial distributions of v, T_s, and flux number of fused and crushed alumina particles in two plasma jets with total flow rates of 60 and 90 slm. It can be seen that, in spite of a higher (37%) velocity with the 90 slm flow rate, the surface temperature is almost the same, even if in the 90 slm flow rate the H_2 mole fraction is only 17% versus 25% in the 60 slm flow rate. This means that, in spite of a slightly shorter plasma jet, a higher velocity, and a lower thermal conductivity,[20] constriction of the plasma jet with the flow rate increase induces a higher gas enthalpy, which maintains the particle surface temperature almost constant.

4.3 *Influence of Hydrogen Percentage in Argon*

With pure argon plasma jets, for the same arc current, the torch voltage is one third that obtained with Ar-H_2 (20 vol%) plasmas, and it is thus difficult to compare both plasma jets due to power level differences. Direct current (dc) spraying plasma torches hardly sustain more than 1000 A with pure Ar and more than 800 A with Ar-H_2 mixtures. However, the argon flow rate can be reduced in such a way that the mean enthalpies of both jets are the same, even if the real enthalpies of the hot plasma columns are probably different due to the higher constriction of the Ar-H_2 plasma. The results for the surface temperature of fused and crushed alumina particles obtained with two plasma jets with the same mean enthalpy are shown in Fig. 16. It can be readily seen that, in spite of a velocity that is twice as low as in the argon plasma, the surface temperature is 10% higher for the Ar-H_2 plasma with 18.5 vol% H_2. This is due to the higher mean thermal conductivity of this mixture, which takes into account the recombination of the H atoms.[20] The influence of the H_2 percentage can also be seen in Fig. 15(b) and in Fig. 17. With 9% H_2 (Fig. 17) versus 17% H_2 (Fig. 15b), the velocities are almost the same, but the surface temperatures are 4 to 5% higher with the 17% H_2 mixture.

4.4 *Comparison of Ar-H_2 and Ar-He Mixtures*

According to Pateyron *et al.*,[20] the mean integrated thermal conductivities of Ar-H_2 (18.5 vol%) and Ar-He (60 vol%) plasmas are about the same (at least for temperatures higher than 9000 K). The viscosity of the Ar-He (60 vol%) mixture is higher (about 55% at the maximum) than that of the Ar-H_2 (18.5 vol%) mixture. Comparison of the plasma jets is as difficult as that between Ar and Ar-H_2 because the maximum voltage with Ar-He is about 40 V versus 70 to 80 V with Ar-H_2. However, even with a lower power level for Ar-He, it was possible to find conditions where both plasma jets have about the same length and diameter.[21] This was achieved by using 75 slm Ar-15 slm H_2 with a power level of 31 kW versus 40 slm Ar-60 slm He with a power

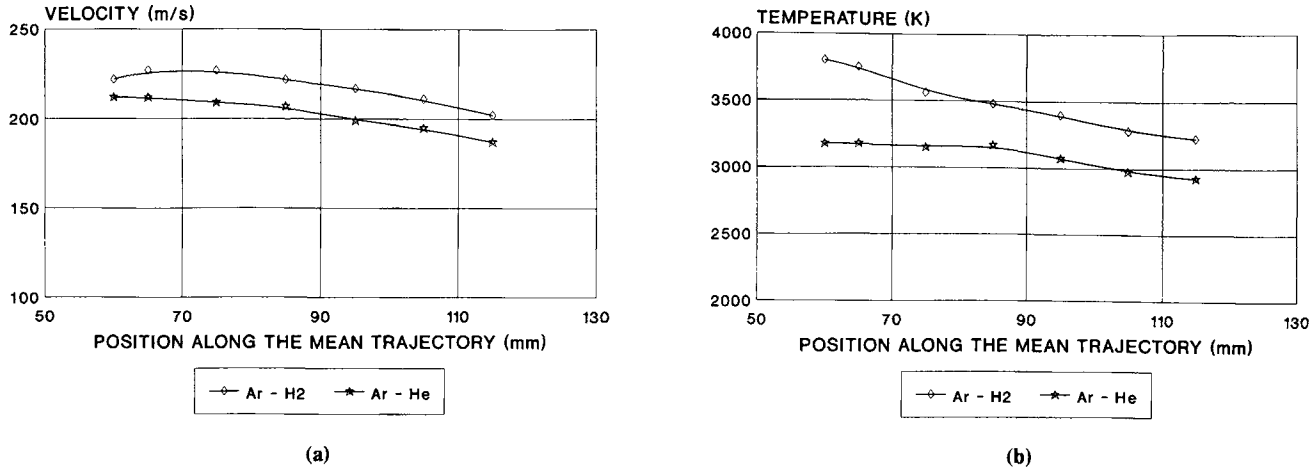

Fig. 18 Evolution along their mean trajectory of the mean velocity (a) and mean surface temperature (b) of ZrO_2 + 8 wt% Y_2O_3 particles (–45+22 μm) injected in an Ar (75 slm)-H_2 (15 slm) plasma jet at 31 kW or in an Ar (40 slm)-He (60 slm) jet at 23.4 kW. In both cases, the nozzle diameter was 8 mm.

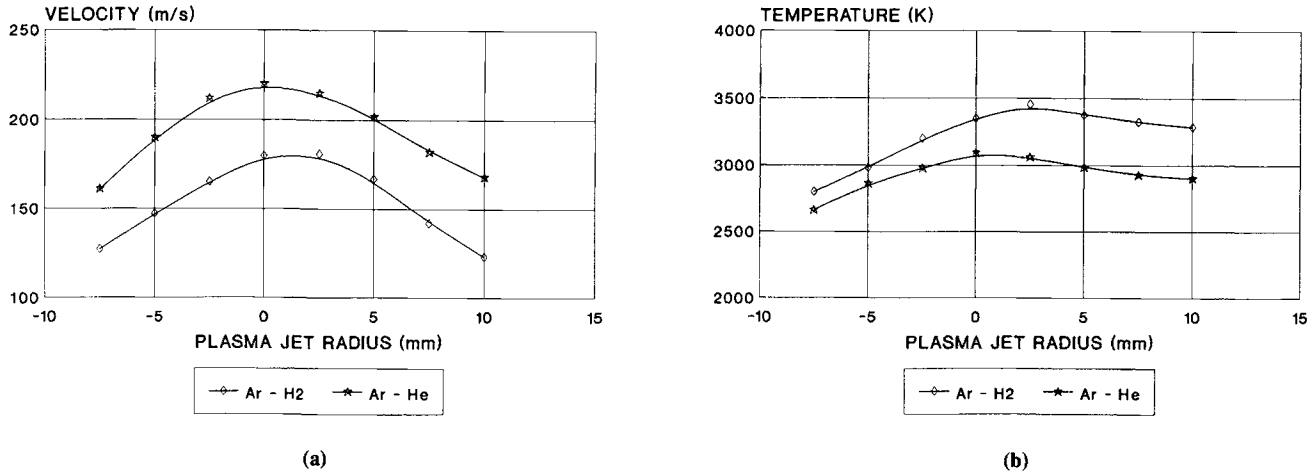

Fig. 19 Radial distributions of velocity (a) and surface temperature (b) measured 75 mm downstream of the nozzle exit for the same conditions as those depicted in Fig. 18, except that the Ar-H_2 power level was lowered to 23.4 kW.

level of 23.4 kW and almost the same arc currents. The Ar-He plasma jet is as long as the Ar-H_2 one because of its higher viscosity, thus reducing the surrounding air pumping. Figure 18 shows the velocity and surface temperature of fused and crushed ZrO_2-8 wt% Y_2O_3 particles (–45+22 μm) along their mean trajectory in both plasma jets. If the velocities are not very different (less than 10%), the surface temperature of the particles in the Ar-H_2 plasma is 800 K higher than that in the Ar-He plasma jet 50 mm downstream of the nozzle exit. This is probably due to the higher enthalpy of the Ar-H_2 jet and to its higher mean thermal conductivity for temperatures lower than 10,000 K. However, with its higher viscosity, particularly at temperatures below 10,000 K, the Ar-He plasma undergoes less mixing with the surrounding air than the Ar-H_2 plasma. Thus, the particle surface temperature decrease with distance is lower with this plasma.

When the power level of the Ar-H_2 plasma jet is reduced to that of the Ar-He plasma, the velocity of the particles in the Ar-H_2 plasma is lower than that obtained in the Ar-He plasma, but the surface temperature is still higher for the Ar-H_2 plasma (see Fig. 19). This figure shows the advantage of heat transfer with Ar-H_2 due to the recombination of H atoms, thus resulting in a higher mean thermal conductivity at $T < 10{,}000$ K.

4.5 *Influence of Nozzle Diameter*

When the nozzle diameter is increased from 6 to 8 mm for a given gas flow rate and type and a given arc current, then the gas velocity and pumping of the surrounding air decrease. The plasma jet length is also minimally increased. The carrier gas flow rates were adjusted to have the same mean trajectory with nozzles of 6, 7, or 8 mm diameter. The net effect of this diameter change on fused and crushed alumina particles (–45+22 μm) is shown in Fig. 20. The maximum velocity is 50% higher with the 6-mm nozzle compared to the 8-mm nozzle. The 7-mm nozzle gives intermediate results. The velocity in the fringes of the jet drops less rapidly with the 8 mm nozzle, which is expected with a larger diameter jet. Similar results are obtained for changes in

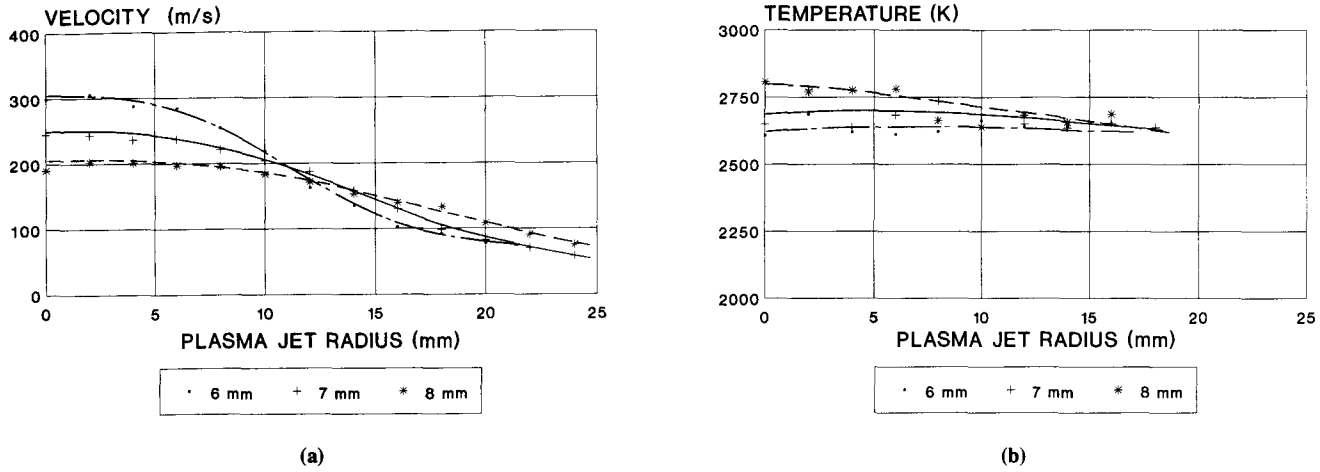

Fig. 20 Radial distribution of velocity (a) and surface temperature (b) measured 75 mm downstream of the nozzle exit for fused and crushed Al_2O_3 particles (–45+22 μm) injected in Ar (45 slm)-H_2 (15 slm) plasma jets with an arc current of 600 A and three nozzle diameters of 6, 7, and 8 mm, respectively.

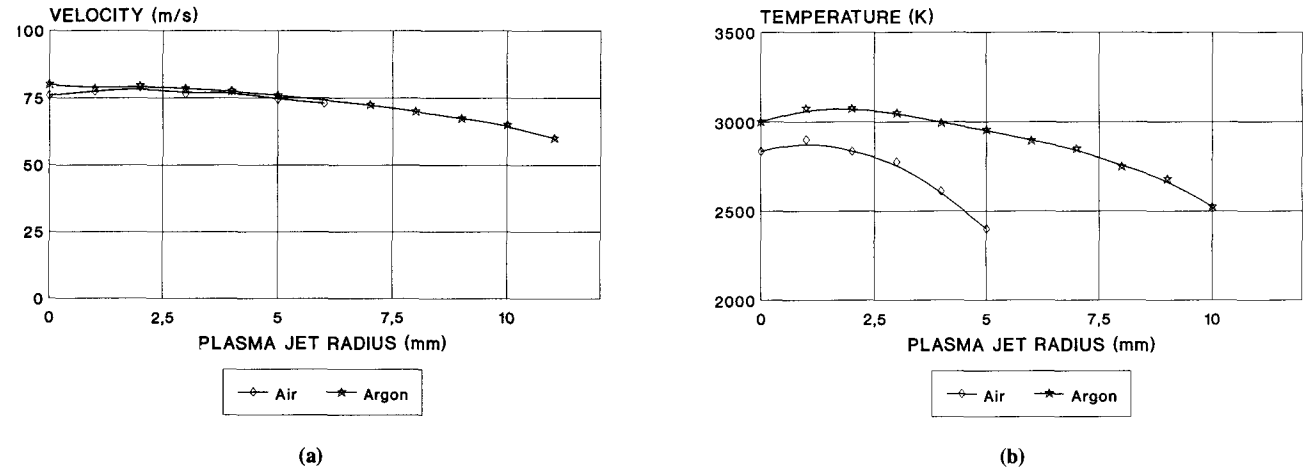

Fig. 21 Radial velocity (a) and surface temperature (b) of nickel particle (–80+60 μm) in an Ar (75 slm)-H_2 (15 slm) plasma jet. P = 29 kW; d = 6 mm flowing in air or in an argon atmosphere.

temperature, the highest values being obtained with the lowest velocity particles, i.e., with the 8-mm diameter nozzle. The results obtained with the 6- and 7-mm nozzle are about the same.

4.6 *Influence of the Surrounding Atmosphere*

When spraying in a controlled atmosphere chamber filled with argon, the plasma jet is broadened and lengthened.[19,22] This is due to the fact that the pumped argon is ionized at 15,000 K, whereas the pumped O_2 from air is dissociated at 3500 K, thus consuming a high quantity of energy even in the fringes of the plasma jet. If the particle velocity is almost the same as that obtained when spraying in air (see Fig. 21a for nickel particles), except that the distribution is broader, then the surface temperature is a little higher (200 K maximum at the measuring distance), but with a much lower drop with respect to the radius when spraying in an Ar atmosphere.

The advantage of spraying in a controlled atmosphere is obvious; however, the cost of the chamber and its utilities is not negligible. Thus, nozzle shields have been developed to delay the mixing of the surrounding air with the plasma jet. Figure 22 shows examples of the normal short PTF4 nozzle (a) and the long nozzle with a shield (b), in which the powder is injected in the exit cone of the nozzle. With this nozzle, the plasma jet exiting is as long as the jet obtained with the normal nozzle in spite of a 25 mm increase in its length. Thus, for comparison purposes, measurements along the mean trajectory for both nozzles are presented, designating the normal nozzle exit as zero. The results obtained for –75+20 μm Y_2O_3 particles are presented in Fig. 23. The velocity of the particles with the shielded nozzle and internal injection is higher than that obtained with the normal nozzle and external injection. It is also worth noting that, due to the lower plasma jet velocity exiting from the diverging section, mixing with the surrounding atmosphere is delayed with the shielded nozzle and the drop in velocity is much lower (230 m/s 120 mm downstream of the nozzle exit versus 130 with the normal nozzle). In spite of the higher velocity, the surface temperature of the particles is also higher with the shielded nozzle, as illustrated in Fig. 23(b).

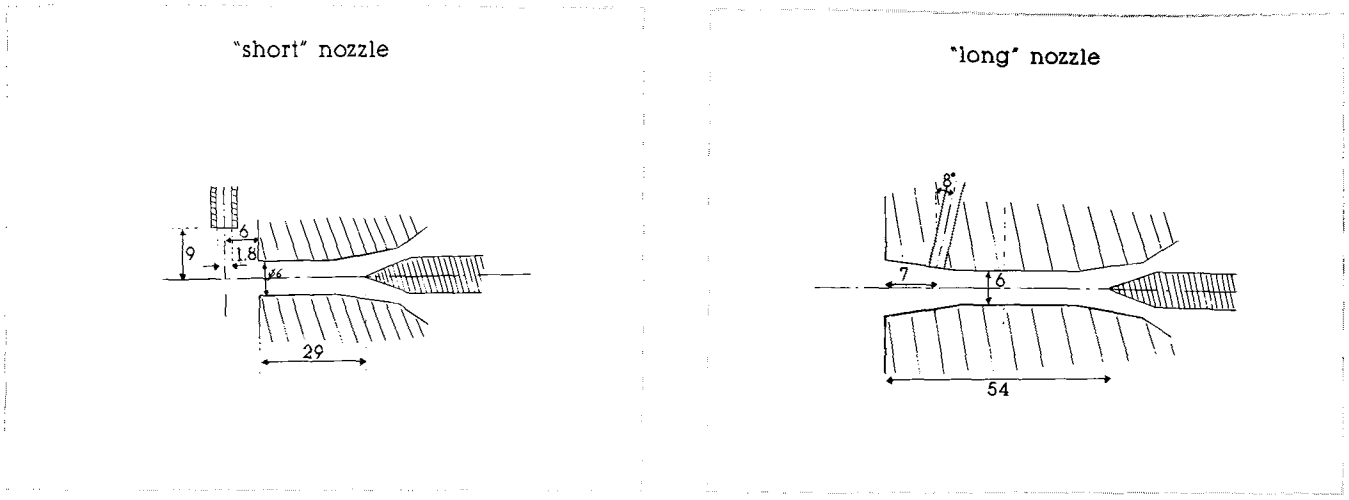

(a) (b)

Fig. 22 Normal PTF4 spraying nozzle (a) and with a shield (b).

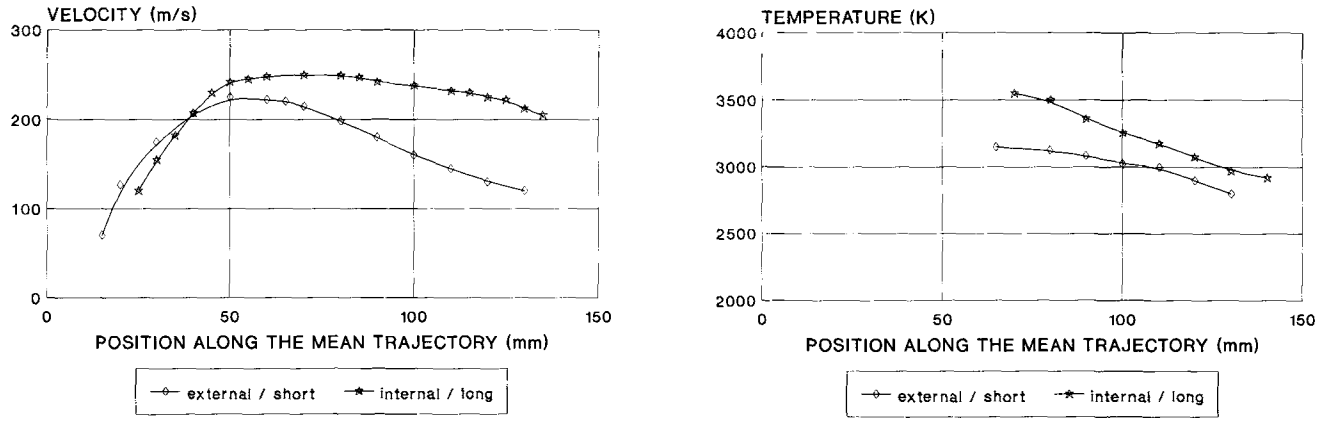

(a) (b)

Fig. 23 Evolution along the mean trajectory of the mean velocity (a) and mean surface temperature (b) of Y_2O_3 particles (–75+20 μm) in the two nozzles shown in Fig. 22 working with 30 slm Ar and 12 slm H_2; P = 31.7 kW.

With the shielded nozzle, the effect of the total gas flow rate (with the same H_2 vol%) varies. Figure 24(a) shows that the velocity increases by 12% when the surface temperature increases by 8% in spite of the higher velocity (Fig. 24b). This shows that the plasma is more constricted by the mass flow rate increase, inducing higher enthalpies and thus higher surface temperatures. With the shielded nozzle, the effect is more pronounced due to the reduced surrounding air pumping that occurs when the gas velocity increases (see for example Fig. 15).

5. Conclusion

Laser anemometry, laser fluxmetry, and statistical two-color pyrometry allow one to obtain velocity, number flux, and surface temperature distributions of in-flight particles of plasma jets and to correlate these values with the macroscopic spraying parameters. However, it is necessary to remember that particles with a surface temperature below 2000 K are not detectable and may be present in regions where measurements show that the particles are molten.

Such measurements have emphasized the importance of the dispersion of the trajectories, dispersion that depends on both the size and injection velocity distributions of the particles. The smaller the particles, the higher the carrier gas flow rate needed to give them the proper momentum, resulting in a broad injection velocity distribution and thus in a broad trajectory distribution inducing different heat treatments. The particles exiting from an injector also exhibit a rather large dispersion angle (up to 30° cone angle) resulting from their collisions with the walls. This dispersion, playing an important role in the trajectory distribution, depends on many parameters (injector inside diameter, carrier gas flow rate, particle size distribution, and density) and is not yet clearly understood. The particle flux measure-

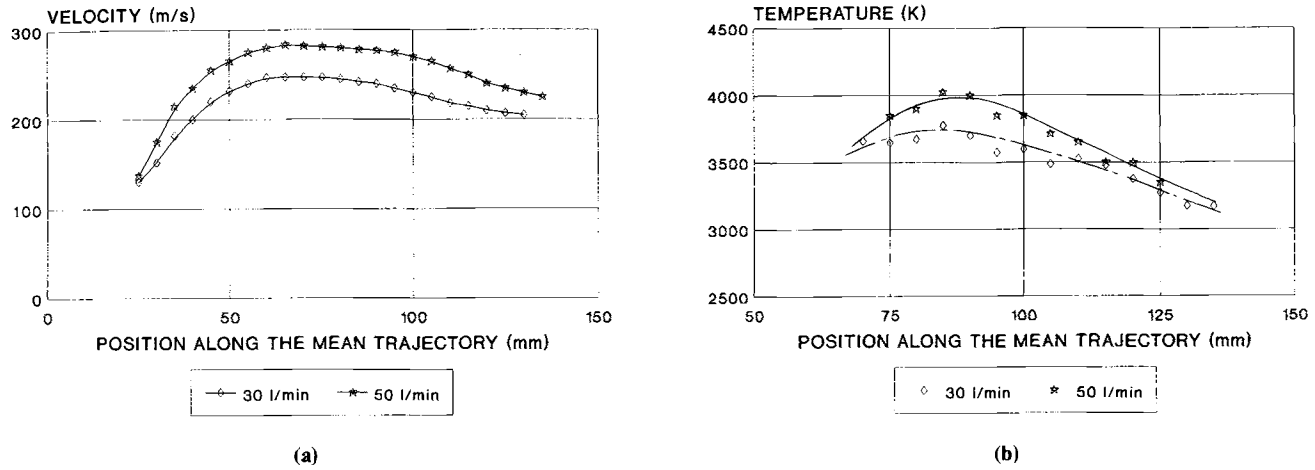

Fig. 24 Evolution along the mean trajectory of the mean velocity (a) and mean surface temperature (b) of Y_2O_3 particles (–75+20 μm) in the two nozzles shown in Fig. 22 working with 30 slm Ar or 50 slm Ar with 30% of H_2 and 31.7 kW.

ments have emphasized the necessity, for a given injector inside diameter, position, and tilting, and for given particles, to adjust the carrier gas to the arc current, nozzle diameter, gas flow rate, and gas type so as to achieve the optimum trajectory to obtain, for example, the best deposition efficiency corresponding to molten particles upon impact. However, the position of the injector and its tilting, as well as the distance from the plasma jet axis, require further studies to improve particle melting, particularly in terms of designs to limit the plasma jet perturbation by the carrier gas.

The influence of the macroscopic parameters on particle melting is strongly linked to the surrounding atmosphere of the plasma jet. Air pumping rapidly cools the plasma jet with oxygen dissociation at 3500 K, and as pumping increases with the plasma gas velocity, all parameters increasing this velocity have a negative effect on particle heating. This happens when the arc current, plasma gas flow rate, or percentage of hydrogen increases, or when the nozzle diameter decreases. On the contrary, when the viscosity of the plasma increases, for example with the He percentage, the pumping effect is reduced. However, the enthalpy of the plasma increases with the arc current, and the heat transfer increases with the hydrogen percentage. Thus, compromises have to be found. For example, to increase the power level (through the arc current) over 40 kW for alumina or zirconia does not increase the surface temperature of the particles because the plasma jet length tends to reach a limit and the velocity increases and reduces the residence time.

For nozzle diameters, a compromise must also be found, the stability of the arc decreases when the diameter of the nozzle increases for a given gas flow rate. To limit the dispersion, larger particles should be injected, but to achieve particle melting, higher percentages of hydrogen should be used to enhance the heat transfer. According to the particles studied (Al_2O_3 and ZrO_2), optimum size for an Ar-H_2 plasma appears to be –45+22 μm. Larger particles are incompletely molten and smaller ones become much too dispersed in the jet. The use of He instead of H_2 limits the surrounding air pumping, but does not melt the particles as well due to the lower thermal conductivity of the mixture. However, the heat propagation phenomenon is less critical, and the particle temperature drops less rapidly than with Ar-H_2. Thus, Ar-He-H_2 mixtures, recently patented, present some advantages for refractory materials spraying.

A controlled atmosphere of argon broadened and lengthened the plasma jet. This results in broader velocity and surface temperature distributions of the particles, with similar maximum velocities but higher temperatures. This of course increases the deposition efficiency. Moreover, in an argon atmosphere, the length of the jet does not tend to reach a limit for $I > 700$ A as when spraying in air, and thus, the surface temperature of the particles increases linearly with arc current. To avoid the cost of a controlled atmosphere chamber nozzle, shields are used to delay the phenomenon of air pumping. Their net effect is to delay the mixing with surrounding air. The velocity of the plasma is lower at the exit of the shield with the conical shape than the velocity at the exit of the normal nozzle, and thus air pumping is reduced. The plasma jet length is about the same as that obtained with the normal nozzle plus the length of the shield for shields that are less than 30 mm in length. Thus, when particles are injected inside the shield, their velocity and temperature are increased. The main problem is that a higher velocity is not necessarily the best for coating properties, and nozzle shields should be used with normal nozzles that provide lower particle velocities to limit the effect of the velocity increase.

Such in-flight measurements have also emphasized the importance of particle morphology and explained why the use of agglomerated particles results in poor mechanical properties of coatings. The agglomerated particles partly explode upon penetration of the plasma, and the small exploded grains traveling in the jet fringes are sucked in by the jet farther downstream and become embedded in the coating. Moreover, particles with diameters greater than 40 μm form hollow spheres with a surface that is overheated and a central core that remains completely unmolten.

If such measurements allow one to optimize the molten state of particles upon impact on the substrate, they are not sufficient to optimize the coating properties, which depend on splat formation and cooling, as well as on the monitoring of temperature gradients within successive passes during spraying. Measurements that allow one to determine the velocity, temperature, and diameter of a single particle upon impact as well as the tempera-

ture evolution during its flattening and the corresponding splat cooling are under development. They will provide interesting information on the coating formation (contact between the splats and substrate or splats and coating) versus the temperature, velocity, and diameter of the impacting particles.

References

1. N.N. Rykalin and V.V. Kudinov, Plasma Spraying, *Pure Appl. Chem.*, Vol 48, 1976, p 229-239
2. J.H. Zaat, Thermal Spraying, *Ann. Rev. Mater. Sci.*, Vol 13, 1983, p 9-42
3. *Thermal Spraying, Practice, Theory and Applications*, American Welding Society, 1985
4. Technology Forecast, *Adv. Mater. Proc.*, Vol 30, 1988
5. P. Fauchais, A. Grimaud, A. Vardelle, and M. Vardelle, Plasma Spraying: A Review, *Ann. Phys. Fr.*, Vol 14, 1989, p 261-310
6. P. Fauchais, J.F. Coudert, A. Vardelle, M. Vardelle, and A. Denoirjean, Diagnostics of Thermal Spraying Plasma Jets, *J. Thermal Spray Technol.*, Vol 1 (No. 2), 1992, p 117-128
7. P. Fauchais, J.F. Coudert, and M. Vardelle, Diagnostics in Thermal Plasma Processing, in *Plasma Diagnostics*, Academic Press, 1989, p 349-446
8. L. Gyenis, A. Grimaud, O. Betoule, F. Monerie-Moulin, P. Fauchais, and M. Ducos, "Influence of Temperature Control during Spraying on Hardness and Cohesion of Alumina Coatings," Proc. 2nd Plasma Technik Symposium, Vol 1, S. Blum-Sandmeier, H. Eschnauer, P. Huber, and A.R. Nicoll, Ed., Wohlen, Switzerland, 1991, p 95-101
9. M. Vardelle, "Study of Heat, Mass and Momentum Transfers Between A dc Plasma Jet and Powders," State thesis, University of Limoges, France, July, 1987
10. M. Vardelle, A. Vardelle, and P. Fauchais, "Experimental Study of the Thermal Exposure Experienced by Powders under Plasma Spraying Conditions in Air and Inert Environment," Proc. 1st Plasma Technik Symposium, Vol 2, P. Huber and H. Eschnauer, Ed., Wohlen, Switzerland, 1988, p 167-178
11. E. Pfender, Particle Behavior in Thermal Plasmas, *Plasma Chem. Plasma Proc.*, Vol 9, 1989, p 167S-194S
12. E. Bourdin, P. Fauchais, and M.I. Boulos, Transient Heat Conduction under Plasma Conditions, *Int. J. Heat Mass Transfer*, Vol 26, 1983, p 567-582
13. G. Schweir, Plasma Spray Powders for TBCs, *Advances in Thermal Spraying*, Pergamon Press, 1986, p 277-286
14. B.A. Kusher, S. Rangaswany, and A.J. Rotolico, "Thermal Spray Powders: Manufacturing Methods and Quality Control Procedures," Proc. 1st Plasma Technik Symposium, Vol 2, P. Huber and H. Eschnauer, Ed., Wohlen, Switzerland, 1988, p 191-202
15. M. Vardelle, A. Vardelle, A. Denoirjean, and P. Fauchais, Heat Treatment of Zirconia Powders with Different Morphologies under Thermal Plasma Conditions, *Mater. Res. Soc. Symp. Proc.*, MRS, 190, 1991, p 175-183
16. D. Bernard, "Plasma Spraying of TBCs," Ph.D. thesis, University of Limoges, France, June 1990
17. E. Lugsheider, I. Rass, H.L. Heijnen, P. Chandler, T. Cosak, P. Fauchais, A. Denoirjean, and A. Vardelle, Comparison of the Coatings Properties of Different Types of Powder Morphologies, *Thermal Spray: International Advances in Coatings Technology*, C.C. Berndt, Ed., ASM International, 1992, p 967-973
18. R. Spores, E. Pfender, Flow Structure of A Turbulent Thermal Plasma Jet, *Surf. Coat. Technol.*, Vol 37, 1989, p 251-260
19. Ph. Roumilhac, J.F. Coudert, and P. Fauchais, Influence of the Arc Chamber Design on the Characteristics and Temperature Distributions of Ar-H_2 and Ar-He Spraying Plasma Jets, *Mater. Res. Soc. Symp. Proc.*, MRS, 190, 1991, p 227-238
20. B. Pateyron, F. Elchinger, G. Delluc, and P. Fauchais, Thermodynamic and Transport Properties of Ar-H_2 and Ar-He Plasma Gases Used for Spraying at Atmospheric Pressure, *Plasma Chem. Plasma Proc.*, Vol 12 (No. 4), 1992, p 421-448
21. Ph. Roumilhac, M. Vardelle, A. Vardelle, and P. Fauchais, Comparison of Heat and Momentum Transfer to Ceramic Particles Sprayed in Ar-He and Ar-H_2 at Atmospheric Pressure, *Thermal Spray Technology: New Ideas and Processes*, D.L. Houck, Ed., ASM International, 1989, p 111-116
22. M. Vardelle, A. Vardelle, Ph. Roumilhac, and P. Fauchais, Influence of the Surrounding Atmosphere under Plasma Spraying Conditions, *Thermal Spray Technology: New Ideas and Processes*, D.L. Houck, Ed., ASM International, 1989, p 117-121